

Vacuum Rabi Spectra of a Single Quantum Emitter

Yasutomo Ota,^{1,*} Ryuichi Ohta,² Naoto Kumagai,¹ Satoshi Iwamoto,^{1,2} and Yasuhiko Arakawa^{1,2}

¹*Institute for Nano Quantum Information Electronics, The University of Tokyo, 4-6-1 Komaba, Meguro-ku, Tokyo 153-8505, Japan*

²*Institute of Industrial Science, The University of Tokyo, 4-6-1 Komaba, Meguro-ku, Tokyo 153-8505, Japan*

(Received 12 November 2014; published 8 April 2015)

We report the observation of the vacuum Rabi splitting of a single quantum emitter by measuring its direct spontaneous emission into free space. We use a semiconductor quantum dot inside a photonic crystal nanocavity, in conjunction with an appropriate cavity design and filtering with a polarizer and an aperture, enabling the extraction of the inherently weak emitter's signal. The emitter's vacuum Rabi spectra exhibit clear differences from those measured by detecting the cavity photon leakage. Moreover, we observe an asymmetric vacuum Rabi spectrum induced by interference between the emitter and cavity detection channels. Our observations lay the groundwork for accessing various cavity quantum electrodynamics phenomena that manifest themselves only in the emitter's direct spontaneous emission.

DOI: 10.1103/PhysRevLett.114.143603

PACS numbers: 42.50.Ct, 42.70.Qs, 78.67.Hc

Cavity quantum electrodynamics (QED) studies the interaction between cavity photons and quantum emitters, such as Rydberg [1] and neutral atoms [2], superconducting qubits [3], nitrogen vacancy centers in diamond [4], and semiconductor quantum dots (QDs) [5–9]. The emitter and cavity photons interact not only with each other at a rate g , but also independently with the free-space vacuum field, leading to irreversible radiation at rates γ (for emitter) and κ (for cavity). When $g \gtrsim \kappa + \gamma$ and the pure emitter dephasing is negligible, the strong coupling regime is achieved and vacuum Rabi splitting (VRS) can be observed in the spectral domain.

In general, the two radiation channels exhibit different spectra, which, in principle, can be separately measured as the emitter VRS spectra $S_{\text{QD}}(\omega)$ and cavity VRS spectra $S_C(\omega)$, as illustrated in Fig. 1(a). Moreover, their interference $S_I(\omega)$ should be expected to affect the measured spectral shape. However, to date VRS spectra have been measured predominantly by cavity transmission, reflection, and emission spectroscopy [2–7], since it is brighter and easier to access for most cavity QED systems. This is particularly the case for QD-based cavity QED systems, since most of these possess high cavity leak rates, such that $\kappa \gg \gamma$.

In atomic cavity QED systems, some spectroscopic studies on the emitter channel have been performed [10] but none of these were performed in the single emitter strong coupling regime. In contrast, theoreticians frequently discuss the emitter spectra [11–18], the importance of which has been discussed pertaining to the study of several intriguing phenomena, including the quantum-classical crossover in single atom lasers [12,19], quantum phase transitions in the Jaynes-Cummings Hubbard model [20], cavity induced transparency [17,21] in low κ systems, and quantum delayed-choice experiments [22]. Importantly, most of these phenomena manifest themselves

only in the emitter spectra. The significance of the interference between the two leakage channels (that has a similarity with Fano interference) has also been addressed in the literature [16,23,24].

In this study, we demonstrate an experimental measurement of VRS by detecting direct spontaneous emission from an emitter into free space, using a single InAs/GaAs QD strongly coupled to a photonic crystal nanobeam cavity. We show that the simple combination of an appropriate cavity design and filtering with both a polarizer and aperture enables the extraction of the emitter channel contribution from the free space radiation field, which is otherwise dominated by the cavity leakage. This technique allows us to isolate and measure the emitter spectra $S_{\text{QD}}(\omega)$ and to compare them with $S_C(\omega)$, as well as to study the interference part $S_I(\omega)$ that provides some asymmetry in the VRS spectra.

We fabricated the photonic crystal nanobeam cavity onto a low density quantum dot wafer grown by molecular beam epitaxy, using a standard combination of electron beam lithography and dry and wet etching. The details of the sample fabrication process can be found in our previous publication [25]. Figure 1(b) shows a scanning electron microscope image of a fabricated device. The cavity is formed at the center of the air-bridge photonic crystal nanobeam by modulating the air hole patterning period [25], and is designed to have a moderate Q factor of 49 000 with suppressed leakage to the vertical direction ($\sim 2\%$ of the total radiation). This suppression is achieved by tuning the number of reflecting air holes [26] and guiding dominant cavity leakage into the side waveguide (see the Supplemental Material, Sec. II [27]). The cavity field distribution overlaid with the cavity design is shown in the inset. For optical measurements, the sample was placed inside a temperature controlled optical cryostat and was kept at 3.1 K throughout the measurement. We use a

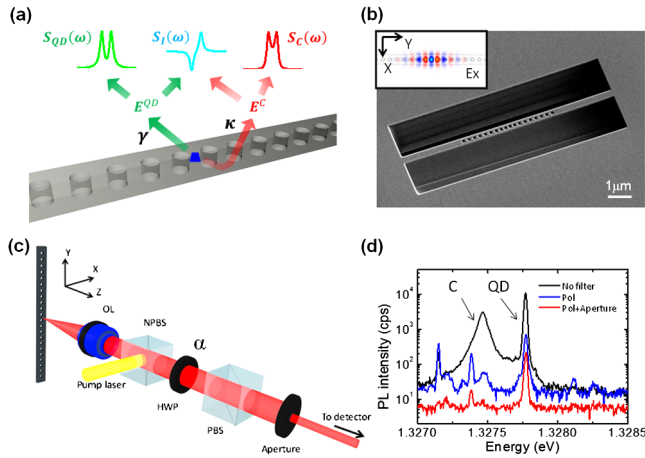


FIG. 1 (color online). (a) Schematic illustration of the photon leakage from our cavity QED system. The direct QD emission into free space excites E^{QD} through the γ channel that results in the QD spectrum $S_{QD}(\omega)$. The cavity also spontaneously radiates and excites E^C from the κ channel, resulting in the cavity spectrum $S_C(\omega)$. Interference between the two leakage channels also occurs, resulting in $S_I(\omega)$. Here, κ and γ include the leakage into both free space and the adjacent waveguide modes, and respectively reflect the total leakage rate of the cavity and emitter. Some part of the leaked photons are directed toward the detector, conceptually placed above the nanobeam cavity. (b) Scanning electron beam micrograph of our device. The inset shows the cavity field distribution overlaid on the cavity design. (c) Schematic of the experimental setup. The sample is addressed by a microscope objective lens (OL) and pumped by a continuous wave laser reflected by the nonpolarized beam splitter (NPBS). The collected light passes through a half wave plate (HWP), polarizing beam splitter (PBS), and an aperture, and is then sent to a spectrometer. The HWP angle α is defined as the angle between the HWP fast axis and the x axis (which is parallel to the horizontal axis of our optical table). (d) μ PL spectra showing the effect of the polarizer and aperture. Without any filtering, a bright cavity peak (C), together with a sharp QD peak (QD), can be seen (black curve). The rotation of the HWP to $\alpha = 50.5^\circ$ strongly suppresses the cavity contribution in the spectrum (blue curve). Further cavity mode suppression can be obtained by the insertion of the aperture (red curve).

continuous wave Ti:sapphire laser oscillating at 860 nm to pump the sample with a fixed power of $7.3 \mu\text{W}$ [except when measuring the spectra shown in Fig. 3(d)]. The pump creates excitons in the QD that radiate as a dipole and finally decay after exciting the electromagnetic field in either the emitter channel, E_{QD} , or cavity channel, E_C , as illustrated in Fig. 1(a). Note that the pump power used is well below the saturation pump power of the QD in resonance with the cavity mode.

We used a microphotoluminescence (μ PL) technique to address the individual sample, with some filters in the detection path, as shown in Fig. 1(c). The pump laser light was focused by an objective lens with a numerical aperture of 0.65, which is also used for collecting radiation from the

sample. Spectra were obtained by a grating spectrometer equipped with a CCD detector placed after the filters (spectral resolution = $13.5 \mu\text{eV}$). A combination of a half wave plate (HWP) at a angle α of 50.5° and a polarizing beam splitter (PBS) enables the rejection of the major cavity far field, which is polarized roughly parallel to the x axis. The aperture, which has a diameter of 0.75 mm and reduces the detection numerical aperture roughly to 0.1, is used to suppress the minor cavity far field, which is polarized orthogonally to the major one (see the Supplemental Material, Sec. III [27]). The effect of these filters on the measured spectrum of a detuned QD-cavity system is shown in Fig. 1(d). Without these filters, strong cavity mode emission is seen (black curve) but it can be largely reduced by the polarization filtering (blue curve). Further reduction is obtained by the aperture (red curve), leading to the near-perfect suppression of the cavity emission that is required to successfully extract $S_{QD}(\omega)$ near the emitter-cavity resonance [which would otherwise be flooded out by $S_C(\omega)$]. In the following measurements, we rotate the HWP to compare the two spectrum components $S_{QD}(\omega)$ and $S_C(\omega)$, but keep the aperture inserted.

First, we measured the effect of emitter-cavity detuning on the emission spectra at two different HWP angles, as plotted in Fig. 2, by tuning the cavity resonant frequency using a Xe gas adsorption technique. When setting $\alpha = 5.5^\circ$, we obtain spectra that mostly emphasize the cavity emission contribution $S_C(\omega)$. This situation is very similar to almost all previous μ PL experiments based on QD-based cavity QED systems. In Fig. 2(a), the cavity-mode-like emission, which forms a diagonal line in the color plot, is visible even under detuned conditions due to off-resonant mode coupling that is prominent in many QD-based systems [7]. An anticrossing of the two emission peaks is clearly observed as the cavity is tuned into resonance with the QD, demonstrating that the system is in the strong coupling regime. In contrast, we observed a

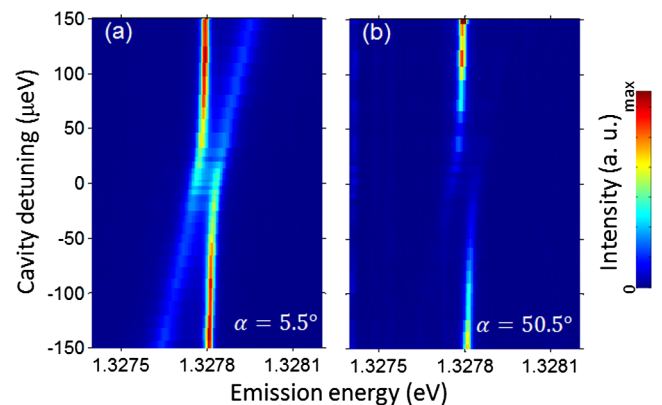


FIG. 2 (color online). (a) Cavity channel spectra under various detunings. α is set to 5.5° . The spectra contain weak contributions from the emitter channel leakage (see text). (b) Emitter channel spectra under various detunings. α is set to 50.5° .

largely different behavior when measuring $S_{\text{QD}}(\omega)$ by setting $\alpha = 50.5^\circ$ [see Fig. 2(b)]. The diagonal cavitylike emission line is not visible under detuned conditions and the total emission intensity significantly decreases as the system is tuned into resonance. This is because $\kappa \gg \gamma$ in our system and the system energy decays dominantly through the cavity channel when near the resonance condition. Nevertheless, we still observe a clear anticrossing in this detection geometry. A detailed comparison of the two sets of spectra in terms of intensities, linewidths, and peak positions can be found in the Supplemental Material, Sec. IV [27].

Now, we discuss the VRS spectra at the resonance. Figure 3(a) shows a normalized resonance spectrum when $\alpha = 5.5^\circ$. This spectrum is dominated by the cavity channel, and clearly shows a vacuum Rabi doublet with a splitting of $64 \mu\text{eV}$. The emission spectra exhibit some asymmetry in that the higher energy emission peak is more intense. The origin of this asymmetry is interference between the cavity leakage field and a minor contribution of the emitter field, namely due to the term $S_I(\omega) = \text{Re}[E_{\text{QD}}^* E_C]$. This contribution from the emitter field arises because our QD is elliptically polarized and its direct spontaneous emission (E_{QD}) cannot be rejected by the polarization filtering, resulting in the fact that we

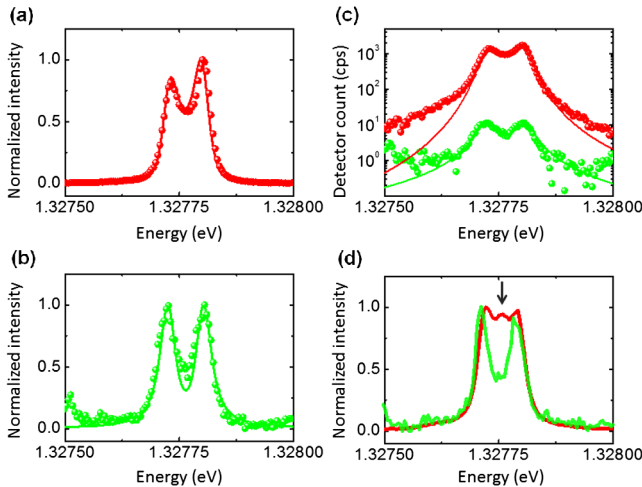


FIG. 3 (color online). (a) Normalized spectra at the resonance measured when mostly emphasizing the cavity leakage contribution ($\alpha = 5.5^\circ$) and (b) when accepting only the emitter channel contribution ($\alpha = 50.5^\circ$). (c) Un-normalized spectra corresponding to (a) and (b). For these three panels, the balls are experimental data and the solid lines are numerical simulations, details of which are presented in the Supplemental Material, Sec. V [27]. (d) Normalized VRS spectra obtained under a 3 times stronger pumping power than in (a)–(c). Red (green) balls are of the mainly cavity (emitter) spectrum. The black arrow indicates the emergence of the additional peak for the cavity leakage channel. Slight asymmetry in the QD spectra is due to unintentional detuning induced by the increase of the pump power.

measure $S_C(\omega) + S_I(\omega)$ (see the Supplemental Material, Secs. I and V [27]). However, by rotating α to 50.5° , we can reject the contribution from the cavity leakage and can solely measure $S_{\text{QD}}(\omega)$, as plotted in Fig. 3(b). The doublet now becomes symmetric and exhibits a deeper central dip than in the mainly cavity spectrum. In addition, the VRS now shows a slightly wider splitting of $75 \mu\text{eV}$ with a wider spectral distribution in the exterior of the doublet. These features are characteristic of VRS spectra of the emitter channel under emitter-driven conditions [13,18]. We note that, since the emitter and cavity photon have a complementarity in this linear strong coupling regime, we should expect that the cavity VRS spectrum under cavity-driven conditions resembles the emitter VRS spectrum under emitter-driven conditions (see the Supplemental Material, Sec. VI [27]).

In these plots, the solid lines show the fitting of the data to our theoretical model, which carefully considers the detection geometry (see the Supplemental Material, Sec. V [27]). In the model, we explicitly consider the pure dephasing of the QD for a better reproduction of the experimental results. Most of the parameters needed for the calculation can be determined experimentally, such as $|g| = 41 \mu\text{eV}$, $\kappa = 66 \mu\text{eV}$ ($Q \sim 20,000$), and $\gamma = 0.28 \mu\text{eV}$, leaving just three free parameters (emitter pure dephasing rate, cavity-free space coupling phase, and degree of $E_{\text{QD}}-E_C$ field overlap). The experimentally obtained parameters accurately reproduce the size of the vacuum Rabi splitting measured through the two detection channels, using formulas derived by Cui and Raymer [13], namely, $2\sqrt{|g|^2 - (\kappa^2 + \gamma^2)}/8 (= 67 \mu\text{eV})$ for the cavity channel and $2\sqrt{[|g|^4 + 2|g|^2\kappa(\kappa + \gamma)/4]^{1/2} - \kappa^2/4} (= 75 \mu\text{eV})$ for the emitter channel. By setting these free parameters to a set of reasonable values, such as a pure dephasing rate of $3 \mu\text{eV}$, we are able to reproduce the experimental results (including those discussed later). Note that, in the model, we fixed the incoherent pumping rate of the QD to be $0.065 \mu\text{eV}$ in order to realize the weak driving condition as in the actual experiments.

Figure 3(c) shows a logarithmic plot of un-normalized resonance spectra for the two detection channels. The peak intensity for the emitter side is roughly 100 times weaker than the other. The simulation clearly reveals the strong asymmetry in the outer sides of the doublet of the mainly cavity spectrum (red). Experimentally, however, the relatively strong background emission hindered observation of this, and the asymmetry is shown by the relative intensities of the doublet peaks.

In Fig. 3(d), we show a spectrum taken under a roughly 3 times higher pumping power than that used for the rest of the experiments. Under this strong pumping condition, an additional peak between the VRS appears in the mainly cavity spectrum (red curve), as indicated by the black arrow. This third peak is often experimentally observed in QD-based cavity QED systems and is believed to arise from

the QD's spectral blinking and also off-resonant cavity feeding [7]. On the other hand, the emitter side (green curve) still exhibits the emission doublet. The contrast between the two spectra further supports the above scenario for the explanation of the origin of the triplet. This result showcases the advantages of our measurement technique for discussing pure VRS spectra without being bothered by the third peak.

Next, we apply our technique to study the influence of the channel interference. We examine how the interference modifies the spectra simply by rotating the HWP and mixing the two channel contributions in a controlled manner. A schematic illustration in Fig. 4(a) explains the details of the experiment. Our elliptically polarized QD couples to free space by exciting the E_x^{QD} and E_y^{QD} fields, while the cavity is assumed to contribute only by its coupling to the E_x^{C} field. By rotating the HWP, we can control the field projection angle Θ , defined with respect to the x axis. Only x -polarized light is transmitted by the PBS, such that the projected field after the PBS is a mixture of the emitter and cavity channel contributions and is expressed as $E = E_x^{\text{C}} \cos \Theta + E_x^{\text{QD}} \cos \Theta + E_y^{\text{QD}} \sin \Theta$.

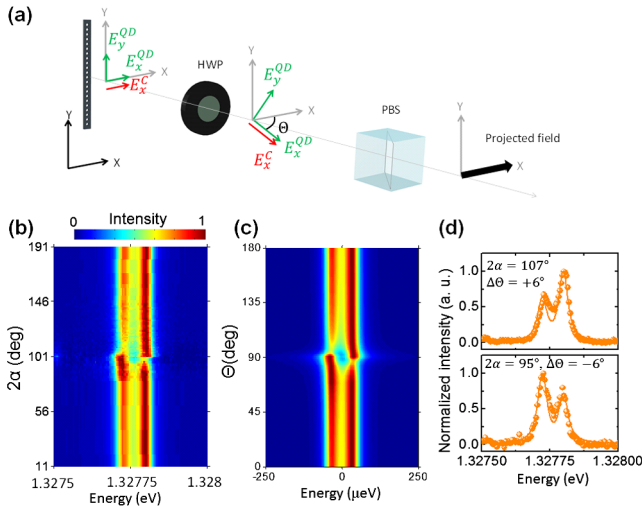


FIG. 4 (color online). (a) Schematic of the interference experiment. The radiation field from the emitter (E_x^{QD} , E_y^{QD}) and cavity (E_x^{C}) pass through the HWP and are projected onto the PBS with an angle Θ . The PBS only allows the transmission of x -polarized light and the resulting field becomes a mixture of the emitter and cavity fields and is expressed as $E = E_x^{\text{C}} \cos(\Theta) + E_x^{\text{QD}} \cos(\Theta) + E_y^{\text{QD}} \sin(\Theta)$. (b) Measured VRS spectra for different HWP angles α . The spectra are mostly modified around $2\alpha \sim 101^\circ$, where the effect of the channel interference is most prominent. Each set of spectra for different α is normalized to its peak. (c) Calculated VRS spectra corresponding to (b). The spectra are calculated for different Θ and are normalized as in (b). (d) Two asymmetric VRS spectra highlighting the effect of channel interference. 2α is set to 95° ($\Delta\Theta = -6^\circ$, lower panel) and 107° ($\Delta\Theta = +6^\circ$, upper panel). Solid lines show the numerical simulation.

The measured spectra are proportional to E^*E , which, thereby, contains Θ -dependent interference terms $\propto \text{Re}[E_x^{\text{C}*}E_x^{\text{QD}}], \text{Re}[E_x^{\text{C}*}E_y^{\text{QD}}]$. When $\Theta = 90^\circ + \Delta\Theta$ with $\Delta\Theta \sim 0$ and using the fact $|E_x^{\text{C}}| \gg |E_y^{\text{QD}}| \sim |E_x^{\text{QD}}|$, the detected field can be approximated as $|E|^2 \sim |E_y^{\text{QD}}|^2 - 2\Delta\Theta \text{Re}[E_y^{\text{QD}*}E_x^{\text{C}}]$, and therefore we will observe both the pure emitter spectrum and a significant contribution from the interference term $\text{Re}[E_y^{\text{QD}*}E_x^{\text{C}}]$. This term is originally zero, since it arises from the orthogonally polarized fields, but becomes finite due to the field projection onto the polarizer.

Figure 4(b) shows a color plot of normalized [micro]PL spectra at resonance taken while varying α from 5.5° to 95.5° , which corresponds to a change of Θ from 0° to 180° . A complicated change in the spectra can be seen, especially around $2\alpha \sim 101^\circ$ ($\Theta \sim 90^\circ$). Numerical calculations for different Θ 's were also performed, and the results are plotted in Fig. 4(c). The agreement between the two sets of spectra is remarkable, and the interference effect is highlighted when 2α is set to 95° ($\Delta\Theta = -6^\circ$) and 107° ($\Delta\Theta = +6^\circ$), as shown in Fig. 4(d). Significantly asymmetric VRS spectra are clearly observed, and the asymmetry flips between $\Delta\Theta = \pm 6^\circ$. This is readily explained by the fact that the interference spectrum is very asymmetric [as illustrated in Fig. 1(a)] and only the sign of its contribution flips when the sign of $\Delta\Theta$ changes. This observation clearly indicates the importance of the channel interference on VRS spectra. We note that the observed spectra contain information of the phase relationship between the cavity, emitter, and the free space. By a comparison to our theoretical model, we estimate the relative phase between the cavity and free space field to be roughly $\sim 0^\circ$ (see the Supplemental Material, Sec. V [27]). This capability to know the cavity and free space relative phase will be valuable for a deeper understanding of open quantum system theories, as it is often hard to theoretically determine its value due to the nontrivial form of the coupling Hamiltonian [35].

In summary, we have measured the VRS spectra of a single quantum emitter and observed spectral modification due to leakage channel interference. We show that a simple combination of an appropriate cavity design, a polarizer, and an aperture is useful for extracting the emitter's direct spontaneous emission into free space, as well as for controlling the interference between the two detection channels. Our demonstration will provide a means to access various intriguing quantum optics phenomena that manifest themselves in only the emitter spectrum, such as the incoherently pumped Mollow triplet, which is predicted to occur when single emitter cavity QED systems start lasing [12,19]. In particular, such phenomena in nonlinear strong coupling regimes of cavity QED are of interest for further experimental studies, since they could be hard to reproduce using many-atom cavity QED systems [10,36].

We hope that our findings will also stimulate discussion on novel cavity QED experiments and theories that use the emitter direct spontaneous emission, which, for example, may act as an novel feedback channel in quantum control.

The authors thank M. Holmes, S. Kako, K. Kamide, and M. Yamaguchi for fruitful discussions. This work was supported by Project for Developing Innovation Systems of the Ministry of Education, Culture, Sports, Science and Technology (MEXT), Japan, and by the Japan Society for the Promotion of Science (JSPS) through its Funding Program for world-leading Innovation R&D on Science and Technology (FIRST Program).

*ota@iis.u-tokyo.ac.jp

- [1] J. Raimond, M. Brune, and S. Haroche, *Rev. Mod. Phys.* **73**, 565 (2001).
- [2] A. Boca, R. Miller, K. M. Birnbaum, A. D. Boozer, J. McKeever, and H. J. Kimble, *Phys. Rev. Lett.* **93**, 233603 (2004).
- [3] A. Wallraff, D. I. Schuster, A. Blais, L. Frunzio, R.-S. Huang, J. Majer, S. Kumar, S. M. Girvin, and R. J. Schoelkopf, *Nature (London)* **431**, 162 (2004).
- [4] Y.-S. Park, A. K. Cook, and H. Wang, *Nano Lett.* **6**, 2075 (2006).
- [5] T. Yoshie, A. Scherer, J. Hendrickson, G. Khitrova, H. Gibbs, G. Rupper, C. Ell, O. Shchekin, and D. Deppe, *Nature (London)* **432**, 200 (2004).
- [6] J. P. Reithmaier, G. Sek, A. Löffler, C. Hofmann, S. Kuhn, S. Reitzenstein, L. V. Keldysh, V. D. Kulakovskii, T. L. Reinecke, and A. Forchel, *Nature (London)* **432**, 197 (2004).
- [7] K. Hennessy, A. Badolato, M. Winger, D. Gerace, M. Atatüre, S. Gulde, S. Fält, E. L. Hu, and A. Imamoglu, *Nature (London)* **445**, 896 (2007).
- [8] D. Englund, A. Faraon, I. Fushman, N. Stoltz, P. Petroff, and J. Vucković, *Nature (London)* **450**, 857 (2007).
- [9] K. Srinivasan and O. Painter, *Nature (London)* **450**, 862 (2007).
- [10] J. J. Childs, K. An, M. S. Otteson, R. R. Dasari, and M. S. Feld, *Phys. Rev. Lett.* **77**, 2901 (1996).
- [11] H. J. Carmichael, R. J. Brecha, M. G. Raizen, H. J. Kimble, and P. R. Rice, *Phys. Rev. A* **40**, 5516 (1989).
- [12] M. Löffler, G. M. Meyer, and H. Walther, *Phys. Rev. A* **55**, 3923 (1997).
- [13] G. Cui and M. C. Raymer, *Phys. Rev. A* **73**, 053807 (2006).
- [14] F. P. Laussy, E. del Valle, and C. Tejedor, *Phys. Rev. Lett.* **101**, 083601 (2008).
- [15] M. Yamaguchi, T. Asano, and S. Noda, *Opt. Express* **16**, 18067 (2008).
- [16] M. Yamaguchi, T. Asano, M. Fujita, and S. Noda, *Phys. Status Solidi C* **5**, 2828 (2008).
- [17] A. Auffèves, B. Besga, J.-M. Gérard, and J.-P. Poizat, *Phys. Rev. A* **77**, 063833 (2008).
- [18] F. P. Laussy, A. Laucht, E. del Valle, J. J. Finley, and J. M. Villas-Bôas, *Phys. Rev. B* **84**, 195313 (2011).
- [19] E. del Valle and F. P. Laussy, *Phys. Rev. Lett.* **105**, 233601 (2010).
- [20] M. Knap, E. Arrigoni, W. von der Linden, and J. H. Cole, *Phys. Rev. A* **83**, 023821 (2011).
- [21] P. M. Alsing, D. A. Cardimona, and H. J. Carmichael, *Phys. Rev. A* **45**, 1793 (1992).
- [22] R. Stassi, A. Ridolfo, S. Savasta, R. Girlanda, and O. D. Stefano, *Europhys. Lett.* **99**, 24003 (2012).
- [23] P. E. Barclay, C. Santori, K.-M. Fu, R. G. Beausoleil, and O. Painter, *Opt. Express* **17**, 8081 (2009).
- [24] K. H. Madsen and P. Lodahl, *New J. Phys.* **15**, 025013 (2013).
- [25] R. Ohta, Y. Ota, M. Nomura, N. Kumagai, S. Ishida, S. Iwamoto, and Y. Arakawa, *Appl. Phys. Lett.* **98**, 173104 (2011).
- [26] A. Enderlin, Y. Ota, R. Ohta, N. Kumagai, S. Ishida, S. Iwamoto, and Y. Arakawa, *Phys. Rev. B* **86**, 075314 (2012).
- [27] See Supplemental Material at <http://link.aps.org/supplemental/10.1103/PhysRevLett.114.143603>, which includes Refs. [28–34] and details of the QD characterization, cavity design, effect of the aperture, detuning dependence of the VRS spectra, theoretical modeling, and emitter-cavity complementarity.
- [28] N. Kumagai, S. Ohkouchi, M. Shirane, Y. Igarashi, M. Nomura, Y. Ota, S. Yorozu, S. Iwamoto, and Y. Arakawa, *J. Phys. Conf. Ser.* **245**, 012088 (2010).
- [29] S. Ohno, S. Adachi, R. Kaji, S. Muto, and H. Sakakura, *Appl. Phys. Lett.* **98**, 161912 (2011).
- [30] L. Mandel and E. Wolf, *Optical Coherence and Quantum Optics* (Cambridge University Press, Cambridge, England, 1995).
- [31] M. Yamaguchi, Ph.D. thesis, Kyoto University, 2010.
- [32] M. O. Scully and M. S. Zubairy, *Quantum Optics* (Cambridge University Press, Cambridge, England, 1997).
- [33] J.-T. Shen and S. Fan, *Phys. Rev. A* **79**, 023838 (2009).
- [34] P. R. Berman, D. R. Bates, and B. Bederson, *Cavity Quantum Electrodynamics* (Academic Press, New York, 1994).
- [35] C. Viviescas and G. Hackenbroich, *Phys. Rev. A* **67**, 013805 (2003).
- [36] Y. Zhu, D. J. Gauthier, S. E. Morin, Q. Wu, H. J. Carmichael, and T. W. Mossberg, *Phys. Rev. Lett.* **64**, 2499 (1990).